Formation of Iron(III)–Tyrosinate Is the Fastest Reaction Observed in Ferritin†

Geoffrey S. Waldo and Elizabeth C. Theil*

Departments of Biochemistry and Physics, North Carolina State University, Raleigh, North Carolina 27695-7622

Received June 17, 1993; Revised Manuscript Received August 23, 1993®

ABSTRACT: Rapid mineralization of ferritin, characteristic of protein with H-type subunits, coincides with formation of a specific Fe(III)–tyrosinate complex. The pseudo-first-order rate constant for Fe(II) oxidation by H-subunit-type ferritin has now been shown to be 700–900 times greater than any previously reported for ferritin; k_{ox} = 1000 s^{-1} for formation of the specific Fe(III)–tyrosinate complex (A_{550nm}) or formation of less defined Fe(III)–oxo multinuclear complexes (A_{420nm}). Formation of multinuclear Fe(III)–oxo complexes and O_2 consumption were biphasic. In the first phase, up to 50 Fe atoms/ferritin molecule were rapidly oxidized, accompanied by formation of the Fe(III)–tyrosinate complex; saturation of the sites which formed the Fe(III)–tyrosinate complex also required 50 Fe/ferritin molecule. The sigmoidal shape of the curve obtained by plotting the initial rate of oxidation during the rapid phase of mineralization *versus* added [Fe(II)] suggested a more complex reaction pathway of ferroxidation than previously described. During the second phase of mineralization, Fe(III)–tyrosinate decreased, but multinuclear Fe(III)–oxo complexes and O_2 consumption continued to increase at a slower rate. Recovery of the rapid oxidation pathway paralleled recovery of the site for Fe(III)–tyrosinate formation; full regeneration of the Fe(III)–tyrosinate sites was gradual over a period of 12 h, as if the movement of Fe(III) along the biomineralization pathway in the protein was slow and was accompanied by conformational changes which affected the Fe(III)–tyrosinate site. The rapid mineralization rates characteristic of ferritin with H-type subunits clearly involves Fe(III)–tyrosinate at a very early, and possibly the first, stop along the route of Fe through the protein coat to the central core.

Ferritin, the highly conserved, ubiquitous Fe storage protein, maintains Fe in a nontoxic, bioavailable form for use in a variety of important biological electron transfer reactions including respiration, photosynthesis, and nitrogen fixation [reviewed in Ford et al. (1984), Theil (1987, 1990), and Harrison and Lilley (1990)]. Up to 4500 Fe atoms in a mineral core are stored within the hollow, spherical protein coat of 24 polypeptide subunits (Theil, 1990; Harrison & Lilley, 1990). The two principal classes of ferritin subunits found in eukaryotes are classified H or L, which define sets of sequences rather than size (Theil, 1990). H-subunit-type ferritin is associated with rapid Fe biomineralization (Levi et al., 1988; Lawson et al., 1989; Wade et al., 1991; Waldo et al., 1993). L-subunit ferritin can still form cores, although at far slower rates (Levi et al., 1988, 1989; Lawson et al., 1991; Waldo et al., 1993).

Ferritin is perhaps unique among known metalloproteins in lacking stable metal sites, since a major role of the protein is guiding Fe(II) in solution outside the protein through the protein coat to the Fe(III)–oxo mineral core, rather than merely binding Fe. A number of metal sites have been observed by X-ray diffraction, using heavier metals to model iron sites (Harrison & Lilley, 1990). X-ray absorption, Mössbauer, and electron paramagnetic resonance (EPR) spectroscopy have identified a number of Fe(III)–oxo species, some bound to protein ligands, such as small Fe(III)–oxo clusters and oxo dimers of Fe(II)/Fe(III) or Fe(III)/Fe(III) that may be intermediates, measuring either Fe itself or using other metals as reporters for Fe binding (Yang et al., 1987; Chasteen et al., 1985; Chasteen & Theil, 1982; Bauminger et al ., 1989, 1991). In addition, VO^{2+} bound to horse spleen ferritin, analyzed by electron nuclear double resonance (ENDOR) spectroscopy, showed couplings from N nuclei tentatively ascribed to histidine (Hanna et al., 1991). Oxidation of Fe(II) initially occurs on the protein, as evidenced by detection of Fe(III)–tyrosinate (Waldo et al., 1993), and suggested by the different products of O_2 reduction for small numbers of added Fe atoms compared to large numbers (Sun & Chasteen, 1992). Once mineralization of the ferritin core has begun, oxidation of Fe(II) may occur on small Fe(III)–oxo clusters and on the mineral surface as well as on the protein (Bauminger et al., 1989; Jacobs et al., 1989; Xu & Chasteen, 1991; Sun & Chasteen, 1992; Rohrer et al., 1987, 1989; Wade et al., 1991). The ferritin core is a hydrated ferric oxide mineral phase of variable crystallinity and composition (Mann et al., 1987; Mackle et al., 1991; Theil & Sayers, 1991; Rohrer et al., 1990).

Ligands proposed as the site of initial ferroxidation, Glu^{58} and His^{61}, related to rapid mineralization of H-subunit-type ferritin and based on Tb and Ca as models for Fe, were shown by site-directed mutagenesis to abolish rapid mineralization in H-subunit-type ferritin (Lawson, 1989, 1991; Bauminger et al., 1992; Treffry et al., 1992). However, the same ligands are also found in a bullfrog ferritin (Dickey et al., 1987), recently shown to have the slow mineralization rates of L-subunit-type ferritin (Waldo et al., 1993). Clearly, these residues alone cannot explain the rapid rate of ferroxidation of H- *versus* L-subunit type ferritins. However, a specific Fe(III)–tyrosinate complex has recently been associated with rapid mineralizing H-subunit-type ferritin; a specific tyrosine conserved in H-type ferritin subunits is absent in L-type ferritin subunits (Waldo et al., 1993).

† This work is supported by NIH Grants R37-DK20251 (E.C.T.) and F32-DK08793 (G.S.W.).

* To whom correspondence should be addressed.

® Abstract published in *Advance ACS Abstracts*, November 15, 1993.

0006-2960/93/0432-13262$04.00/0

The purple Fe(III)–tyrosinate complex in H-subunit-type ferritin provides the first opportunity to follow a specific, chromophoric, Fe–protein intermediate during the mineralization process (Waldo et al., 1993). Prior to the identification of the Fe(III)–tyrosinate complex in H-subunit ferritin by resonance Raman spectroscopy (Waldo et al., 1993), no specific amino acid in ferritin had been identified bound to Fe(III). In this study the kinetic properties of formation of the Fe(III)–tyrosinate complex were studied and compared to those of the less defined, but frequently measured, multinuclear Fe(III)–oxo complexes, using ultraviolet–visible stopped-flow spectroscopy; rates of consumption of O_2 were also analyzed. The results showed a very rapid burst of oxidation of a discrete number ($n \sim 50$) of Fe atoms/ferritin molecule early in the biomineralization of ferritin composed of H-type subunits. The burst of oxidation clearly involved the purple Fe(III)–tyrosinate complex.

MATERIALS AND METHODS

Bullfrog red cell H-subunit-type ferritin (Didsbury et al., 1986), overexpressed in *Escherichia coli*, was isolated and purified as previously described (Waldo et al., 1993). The purity of the H-subunit-type ferritin was confirmed by electrophoresis in denaturing (SDS) and native gels. The protein as isolated contained <1 Fe atom/ferritin molecule, as determined by a reductive *o*-phenanthroline–Fe(II) assay after protein denaturation (Rohrer et al., 1989). Removal of endogenous Fe by reductive chelation with thioglycolic acid (Chasteen & Theil, 1982) was unnecessary, minimizing the possibility of modification of key residues. Bovine liver catalase (EC 1.15.1.1) and horse spleen ferritin were purchased from Boehringer Mannheim GmbH. Fe was removed from the horse spleen ferritin as previously described (Chasteen & Theil, 1982). The horse spleen apoferritin thus prepared contained <1 Fe atom/ferritin molecule as determined by a reductive *o*-phenanthroline–Fe(II) assay on denaturated protein (Rohrer et al., 1989). Ferritin protein concentrations were determined by the Lowry method (Lowry et al., 1951).

Oximetry experiments (Figure 1A) were performed in a thermostated lucite cell (25 °C) equipped with an YSI Model 5357 microoxygen electrode (Clark type) interfaced to a microcomputer through a Keithley 427 current-to-voltage amplifier and Metrabyte DAS8 analog-to-digital converter board. Gas bubbles were displaced from above the sample in the 150-μL reaction cell with a tight-fitting stopper, through which a small port was drilled to allow microliter injections of reagents via a Hamilton syringe. To eliminate the unacceptably long response time (>6 s for 90% response) obtained with conventional membranes, the electrode was fitted with a 6-μm polypropylene membrane (90% response time of 1 s, as determined by injection of argon-purged water). Prior to each experiment, the electrode was calibrated against air-saturated water and 0.05 M sodium sulfite. In a typical O_2 uptake experiment, 2.08×10^{-6} M apoferritin in 0.1 M MOPS buffer, pH 7.00, containing 0.2 M NaCl was placed in the rapidly stirred cell and allowed to equilibrate for 5 min. Reactions were initiated by microliter additions of Fe(II) (as $FeSO_4$) in 0.05 M HCl. Fe loadings ranged from 6 to 384 Fe(II) atoms/apoferritin molecule (24 subunits/protein).

To facilitate direct comparison of ultraviolet–visible spectral changes with O_2 uptake, a thermostated (25 °C) magnetically stirred 1-cm path length quartz cuvette was fitted with a polyethylene stopper drilled with ports to accept the oxygen electrode and to allow the addition of reagents. Ultraviolet–visible spectra spanning 400–650 nm were measured at 1-s intervals with an HP-8452A diode array spectrophotometer interfaced with a microcomputer.

Rapid kinetic data, necessary for the calculation of initial rates of formation of the Fe(III)–tyrosinate complex, were measured with a KinTek Instruments ultraviolet–visible stopped-flow spectrophotometer (Johnson, 1986). The instrument had a dead time of <2 ms. The two equal-volume reagent syringes, mixing cell, and 2.5-cm path length cuvette were contained within a thermostated (25 °C) jacket. One syringe was filled with all reagents except Fe(II); the second syringe contained Fe(II) (as $FeSO_4$) in 1 mM HCl. The final working concentrations of all reagents after mixing were identical to those used in the O_2 uptake experiments (*vide supra*). The pH change upon mixing was negligible. Time course absorbance data were measured for multinuclear Fe(III)–oxo complexes at 420 nm (Figure 1B) and for Fe(III)–tyrosinate at 550 nm (Figure 1C). Although the absorbance of Fe(III)–oxo multinuclear complexes is facilitated at 310 nm, a wavelength often used by other workers (typical values are 10-fold larger than those at 420 nm), 310 nm is so close to the intrinsic absorbances of protein tyrosine and tryptophan residues (280 nm) that results could be confounded by conformational changes in the protein. To obtain initial rates, absorbances were recorded at 0.75-ms intervals during the first 0.3 s of the reaction. Data from 15 replicates were averaged at each Fe(II) concentration, and initial rates were determined by fitting a cubic polynomial to the initial region of each progress curve (insets, Figure 2). Two independent preparations of protein were used. Initial rates were taken as the slope at $t = 0$ s. Since the initial rates varied nearly 30-fold over the span of [Fe(II)] examined, optimal fitting regions ranged from 0.2 s at 2.5×10^{-5} M Fe(II) to 0.025 s at 8.0×10^{-4} M Fe(II).

V_{max}, measured as change in absorbance per second, ΔA s^{-1}, was converted to k_{ox}, moles of Fe oxidized per second per mole of ferritin as follows. Molar extinction coefficients were calculated at 550 and 420 nm on a per-Fe basis. For example, using the saturation curve for Fe(III)–tyrosinate formation, Figure 3A, a molar extinction coefficient was calculated; $\epsilon_{550nm} = 22\,300 \pm 500$ M^{-1} cm^{-1}, or 446 ± 10 M^{-1} Fe^{-1} cm^{-1} on a per-metal basis (the formation of Fe(III)–tyrosinate saturated at ca. 50 Fe/ferritin molecule). Molar extinction coefficients on a per-metal basis, ϵ_{420nm} (M^{-1} Fe^{-1} cm^{-1}) were determined from the total absorbance change at 200 s (see Figure 1B) and plotted against the Fe/ferritin ratio. A second-order polynomial was fitted to the data ($r^2 = 0.999$) and extrapolated back to 0 Fe loading to obtain $\epsilon_{420nm_0} = 240 \pm 10$ M^{-1} Fe^{-1} cm^{-1}, the molar extinction per Fe(III) in the limit of small core; such an approach is reasonable given the small amount of core formed during the first 50–100 ms of ferroxidation. Finally, V_{max}, ΔA s^{-1}, was converted to moles of Fe oxidized per second per mole of ferritin using the per-metal molar extinction coefficients for the appropriate wavelength, *viz.* k_{ox} (s^{-1}) = V_{max} (ΔA s^{-1})/[[ϵ_{420nm_0} (M^{-1} Fe^{-1} cm^{-1})](2.08 × 10^{-6} M ferritin)]. Long-term progress curves were measured for 200 s at 1-s intervals and data from three replicates were averaged (Figure 1B,C). To accurately determine the maximum amount of Fe(III)–tyrosinate formed during the reaction (Figure 3A) (A_{550nm} maximized at ca. 1–3 s after mixing, Figure 1C), the absorbance at 550 nm was recorded every 12.5 ms for the first 5 s of the reaction. The various kinetic parameters (i.e., rate constants, Hill parameters) were obtained by linear and nonlinear least-squares (Levenberg–Marquardt) fits of the kinetic data.

The stoichiometry of Fe(II) oxidation was compared for horse spleen ferritin (slow mineralizing) and H-subunit-type ferritin (fast mineralizing) at several Fe/protein ratios (Figure 3B). Different ratios of Fe/protein were achieved at constant [Fe(II)] = 1.0×10^{-4} M, by varying the protein concentration from 1.66×10^{-5} to 1.04×10^{-7} M. This ensured that the observed Fe/O_2 stoichiometries reflected changes in Fe/ferritin ratios and not simply changes in [Fe(II)].

Restoration of the site which forms Fe(III)–tyrosinate (Figure 4) was followed by measuring the absorbance at 550 nm during the burst of oxidation when a second addition of 48 Fe(II) atoms (n = 48/protein molecule) was made to H-subunit-type ferritin which had been incubated for various times after the addition of an initial sample of 48 Fe(II) atoms (n = 48/protein molecule); the working concentrations of protein and iron were identical to those used in the oximetry experiments (*vide supra*). Samples of ferritin were withdrawn from the reaction vessel periodically and placed in either the O_2 electrode cell or a rapidly stirred quartz cuvette before addition of the second bolus of Fe(II). The magnitude of the burst of oxidation was calculated by fitting a straight line to the first 12 s of the second phase of the O_2 uptake data and extrapolating to the time of Fe(II) addition. The amount of the concomitant Fe(III)–tyrosine generated was obtained from the maximum increase in absorbance at 550 nm. The burst of O_2 consumption and the amount of Fe(III)–tyrosinate formed after the second bolus of Fe(II) was added were reported as relative percentages of the values obtained when Fe(II) was added to apoprotein. The spectrophotometer was zeroed using the Fe-loaded protein sample.

RESULTS

Progress Curves for O_2 Consumption, Fe(III)–Oxo Multinuclear Complex Formation, and Fe(III)–Tyrosinate Formation. Earlier studies of O_2 uptake during Fe(II) oxidation by ferritin used slow mineralizing horse spleen ferritin (Xu & Chasteen, 1991; Sun & Chasteen, 1992). For Fe loadings of <50 Fe/ferritin with 8.3×10^{-6} M ferritin, Fe(II) oxidation by horse spleen ferritin required ca. 1 min for completion (Sun & Chasteen, 1992). In contrast, even at a lower protein concentration (2.08×10^{-6} M), Fe(II) oxidation by rapid mineralizing H-subunit-type ferritin was complete in a single phase lasting 3–10 s (Figure 1A) when Fe(II) was added at ratios of Fe/protein ≤50. At higher ratios of Fe/protein, two phases were observed, the initial rapid phase and an additional slower phase (Figure 1A). To facilitate comparison of our results with previous studies of ferritin mineralization, Fe(II) oxidation by H-subunit-type ferritin was also measured at 420 nm [Fe(III)–oxo multinuclear complex formation]. Stopped-flow spectroscopy was required because of the rapidity of the early phase of the reaction with H-subunit ferritin; the same conditions were employed as in the O_2 uptake experiments (Figure 1B). Progress curves were obtained with similar shapes whether O_2 uptake or A_{420} was measured (compare Figure 1, panels A and B). In either case, extrapolation of a straight line fitted to the first 12 s of the second phase of each progress curve suggested that the initial rapid burst of Fe(II) oxidation was saturated at a ratio of Fe/protein of approximately 50. Additional experiments were performed with protein concentrations of 5.2×10^{-7} and 4.16×10^{-6} M (data not shown). The absolute magnitude of the burst (total O_2 consumed or change in A_{420} during the rapid phase) was directly proportional to protein concentration as long as the ratio of Fe/protein was >50. Excess O_2 was present throughout each experiment (see Figure 1A); however, the possibility existed that the kinetics of the reaction, and thus the magnitude of the burst, might be limited by ambient O_2 ($[O_2] = 2.5 \times 10^{-4}$ M for air-saturated water at 25 °C).

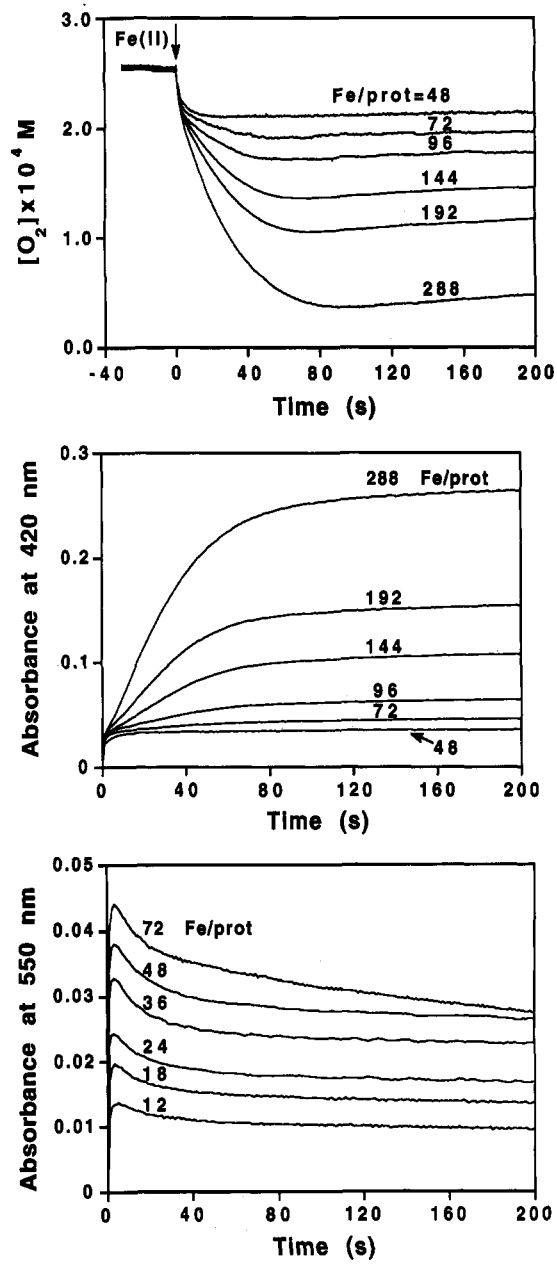

FIGURE 1: Progress curves for the ferroxidation of Fe(II) by H-subunit-type ferritin as a function of Fe(II) loading, [Fe(II)/ferritin molecule], measured by oximetry and ultraviolet–visible spectrophotometry. Conditions: [ferritin] = 2.08×10^{-6} M, 0.20 M NaCl and 0.10 M MOPS, pH 7.00, at 25 °C. (A, top panel) Consumption of O_2 measured by oximetry. The initial burst phase of Fe(II) oxidation is extremely rapid at all Fe(II)/ferritin ratios. All of the Fe(II) is oxidized in a single phase for ratios of Fe/protein ≤ 50 Fe(II)/ferritin. Progress curves are biphasic for ratios of Fe/protein > 50 Fe(II)/ferritin. Extrapolation of the second phase back to the time of Fe(II) addition suggests that approximately 50 Fe(II) atoms per ferritin molecule are oxidized in the burst. (B, middle panel) Fe(III)–Oxo multinuclear complex formation measured at 420 nm by ultraviolet–visible stopped-flow spectroscopy. Approximately 50 Fe(II) atoms per apoferritin molecule appear to be oxidized in the burst. (C, bottom panel) Fe(III)–tyrosinate formation (λ_{max} = 550 nm) measured by ultraviolet–visible stopped-flow spectroscopy. Reaction conditions are the same as for panel A. Fe(III)–tyrosinate concentrations rapidly reach a maximum during the initial burst of oxidation and then gradually decrease during the second slower phase of oxidation, in contrast to O_2 consumption and Fe(III)–oxo multinuclear complexes. Note the apparent decrease in stability of the Fe(III)–tyrosinate at >50 Fe(II)/ferritin.

Therefore, the effect of varying $[O_2]$ was investigated at the highest [Fe(II)] employed (8.0×10^{-4} M); $[O_2]$ of 1.25×10^{-4} and 5.0×10^{-4} M had no effect on the magnitude of the burst.

In order to determine the relationships of the formation of the purple Fe(III)–tyrosinate complex to oxygen uptake and Fe(III)–oxo multinuclear complex formation, A_{550nm} was followed by stopped-flow spectroscopy under the same conditions employed in measuring Fe(III)–oxo multinuclear complex formation (A_{420nm}). Formation of the Fe(III)–tyrosinate complexes parallels oxygen uptake and formation of Fe(III)–oxo multinuclear complexes in the early rapid phase of biomineralization (Figure 1A–C), but the decay[1] of Fe(III)–tyrosinate during the second phase of oxygen uptake suggests that the Fe(III)–tyrosinate complex is a precursor of the mature mineral formed in H-type ferritin. The data further suggest that the initial rapid burst associated with H-subunit ferritin biomineralization occurs on the protein.

Initial Rate of Oxidation: Formation of Fe(III)–Tyrosinate and Fe(III)–Oxo Multinuclear Complexes. Initial rates of Fe(III)–tyrosinate (A_{550nm}) and Fe(III)–oxo multinuclear cluster formation (A_{420nm}) are shown plotted *versus* [Fe(II)] (Figure 2). The initial rates were obtained from cubic fits (see Materials and Methods) to the progress curves (insets, Figure 2). The initial rates were directly proportional to protein concentration. Evidence that the data were collected under saturating $[O_2]$, is the observation that halving the $[O_2]$ at the highest [Fe(II)] concentration used [8.0×10^{-4} M Fe(II)] had no discernible effect on the initial rate. The rate plots are sigmoidal (Figure 2). Lineweaver–Burk plots (1/rate *versus* 1/[Fe(II)]) showed pronounced curvature with decreasing [Fe(II)]; however, plots of 1/rate *versus* $1/[Fe(II)]^2$ were linear ($r^2 = 0.9995$ and 0.9996 for A_{550} and A_{420} data, respectively), suggesting cooperative pairwise binding of Fe(II) (Segel, 1975). Raw initial rates were fit directly to the Hill equation (Hill, 1910):

$$\frac{V}{V_{max}} = \frac{[Fe(II)]^{n_{app}}}{K_{app} + [Fe(II)]^{n_{app}}} \quad (1)$$

by refining V_{max}, n_{app}, and K_{app}, where V is the observed initial rate, V_{max} is the rate at saturating [Fe(II)], n_{app} is the Hill parameter [the apparent number of cooperative Fe(II) binding sites], and K_{app} is the apparent dissociation constant for Fe(II) binding. The fits are shown in Figure 2, and the refined kinetic parameters are summarized in Table I.

The pseudo-first-order rate constant of formation of Fe(III)–tyrosinate during the rapid phase of Fe(II) oxidation by H-subunit-type ferritin, $k_{ox} = 920 \pm 50$ s^{-1}, is ca. 700 times larger than the rate constant for Fe(II) oxidation measured by O_2 consumption for horse spleen ferritin comprised of 15% H-type subunits, 1.3 ± 0.05 s^{-1} (Sun & Chasteen, 1992). Even when corrected for the relative percentages of H-subunit in the two proteins, k_{ox} is still 100 times larger. The Fe(III)–tyrosinate complex formation rate constant for the rapid ferroxidation path in H-subunit-type ferritin is characteristic

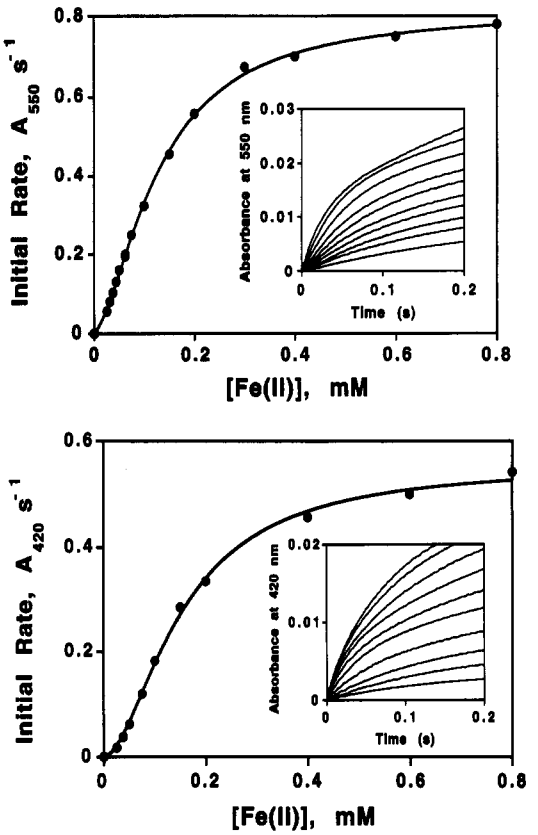

FIGURE 2: Initial rates of Fe(II) oxidation during ferroxidation by H-subunit-type ferritin, measured by ultraviolet–visible stopped-flow spectroscopy *versus* initial [Fe(II)]. Reaction conditions were as described in Figure 1. (A, top panel) Initial rates of formation of Fe(III)–tyrosinate, reported in units of ΔA_{550} s^{-1}. The sigmoidal curve is fit to the Hill equation, with Hill parameter $n_{app} = 1.6 \pm 0.1$ (see Results). (B, bottom panel) Initial rates of Fe(III)–oxo multinuclear complex formation, ΔA_{420} s^{-1}. Curve is fit to Hill equation, $n_{app} = 1.8 \pm 0.1$. Kinetic parameters from fits of the Hill equation to the data for Fe(III)–tyrosinate and Fe(III)–oxo multinuclear complex formation are summarized in Table I. (Insets) Representative progress curves, each an average of 15 transients. In general, progress curves were too complex to be modeled as a single-exponential process; therefore initial rates (ΔA s^{-1}) were determined by fitting a cubic polynomial to the first part of each progress curve.

of product formation rate constants in "typical" enzymes, i.e., 10^3 s^{-1} (Fersht, 1975).

Stoichiometry of Fe(III)–Tyrosinate Formation. Progress curves for O_2 uptake (Figure 1A) and Fe(III)–oxo multinuclear complex formation (Figure 1B) suggest that the initial rapid burst involves a ratio of 50 Fe/protein. However, since only Fe(III)–tyrosinate formation measures a specific Fe–protein complex, determining the stoichiometry of the Fe(III)–tyrosinate complex would clarify whether all of the rapid burst of iron oxidation is occurring on the protein. At low Fe/protein ratios, the amount of Fe(III)–tyrosinate formed is proportional to the number of Fe(II) atoms oxidized in the burst but reaches saturation at higher ratios of Fe/protein (Figure 3A). From the intersection of straight lines fitted to and extrapolated from these regions, it is clear that Fe(III)–tyrosinate formation saturates at ca. 50 Fe/ferritin (Figure 3A); the same value was obtained from the rapid burst of oxygen uptake and Fe(III)–oxo multinuclear cluster formation. Thus, essentially all of the iron oxidation associated with the rapid burst occurs on the protein. An estimate of the number of tyrosines involved in the Fe(III)–tyrosinate complex can be obtained by comparison of the extinction coefficient for Fe(III)–tyrosinate in ferritin (450 M^{-1} cm^{-1} Fe^{-1}) to that in other Fe(III)–tyrosine proteins [ϵ_{max} = 1200–4000 M^{-1} cm^{-1}

[1] The observed biphasic decrease in A_{550nm} probably reflects differing rates of dissociation of Fe(III) from the tyrosine (Figure 1C). Dissociation of a subset of the initial Fe(III)–tyrosinate complexes during the rapid phase of A_{550nm} decay might partially block a common pathway for Fe migration or cause stabilizing conformational changes, thus reducing the rate of decay of the remaining Fe(III)–tyrosinate complexes. Alternatively, the initial rapid decrease in A_{550nm} might reflect a decrease in the extinction coefficient of the Fe(III)–tyrosinate complex, caused by conformational changes upon movement of some Fe which is not directly bound to tyrosine.

Table I: Kinetic Parameters for Ferroxidase Activity in Ferritin Composed of Recombinant H-type Subunits Compared to Horse Spleen Ferritin (H:L ~ 0.15)

	H-subunit-type ferritin[a]		
parameter	Fe(III)–tyrosinate $A_{550\ nm}$	multinuclear cluster $A_{420\ nm}$	horse spleen ferritin (H:L ~ 0.15) oximetry
n_{app}	1.6 ± 0.1[b,c]	1.8 ± 0.1[b,c]	not determined
k_{ox}	920 ± 50[b,d,e]	1050 ± 50[b,d]	1.3 ± 0.05[f]

[a] The sequences cloned were from bullfrog red cell ferritin H subunits, but recently the appearance of Fe(III)–tyrosinate (A_{550}) has been observed in recombinant human liver H-chain ferritin (Bauminger et al., 1993). [b] Parameters optimized from nonlinear least-squares fits of the Hill equation (see Results) to the raw initial data (Figure 2). k_{ox} is reported as moles of Fe(II) oxidized per second per mole of H-subunit-type apoferritin protein. K_{app}, the apparent dissociation constant of Fe(II) binding, is (2 ● 0.3) × 10^{-7} M for Fe(III)–tyrosinate and (6 ± 1) × 10^{-7} M for Fe(III)–oxo multinuclear complex formation. [c] n_{app} is the Hill coefficient, the apparent number of sites acting cooperatively for Fe(II) binding. Although the values obtained could mean cooperative binding of at least two Fe(II), in a complex multisubunit protein such as ferritin, the n_{app} could also mean pairs of highly cooperative intersubunit or intrasubunit Fe binding sites. [d] Pseudo-first-order rate constants for Fe(II) oxidation, reported as moles of Fe(II) oxidized per second per mole ferritin (24-mer concentration) at saturating [Fe(II)]. Since the number of ferroxidase sites is unknown, rate constants are reported on a 24-mer basis, in analogy to the calculations of Sun and Chasteen (1992) for horse spleen ferritin. V_{max}, in units of absorbance change per second, was refined from fits to the Hill equation (see Figure 2): $V_{max,550nm}$ = 0.85 ± 0.06 $\Delta A\ s^{-1}$; $V_{max,420nm}$ = 0.55 ± 0.03 $\Delta A\ s^{-1}$. V_{max} was subsequently converted to moles of Fe oxidized per mole of ferritin per second *viz.* for Fe(III)–oxo multinuclear cluster formation $k_{ox}\ s^{-1} = V_{max}\ (\Delta A\ s^{-1})/[(\epsilon_{420\ nm_0})(2.08 \times 10^{-6}$ M ferritin)]; $\epsilon_{420\ nm_0}$ is the molar extinction of coefficient at 420 nm on a per-metal basis, 240 ± 10 $M^{-1}\ Fe^{-1}\ cm^{-1}$ (see Results). [e] Pseudo-first-order rate constant for oxidation of Fe(II) associated with formation of Fe(III)–tyrosinate. Since the actual number of Tyr residues involved in the cluster is unknown, the rate constant of Fe(III)–tyrosinate formation, calculated using $\epsilon_{550\ nm}$ = 446 ● 10 $M^{-1}\ Fe^{-1}\ cm^{-1}$, provides an upper estimate as it assumes that all 48–50 Fe oxidized in the burst are coordinated to Tyr. The same rate constant would be obtained where two Fe were coordinated to each of 24 Tyr or one Fe was bound to each of 48 Tyr. However, if one Fe(III)–O–Fe(III) dimer formed per subunit, with Tyr bound to only one Fe per Fe(III)–O–Fe(III) dimer, the actual rate constant for Fe(III)–tyrosinate formation would be *half* the value reported. [f] Data from Sun and Chasteen (1992). Kinetic measurements based on oximetry for hose spleen ferritin are sufficiently accurate because of the slow rates of oxidation compared to ferritin composed entirely of H-type subunits. Rate constant is reported as moles of Fe(II) oxidized per second per mole of horse spleen ferritin.

Fe^{-1} (Que, 1983)]. Given, the facts that Fe(III)–tyrosinate sites in ferritin are saturated with 50 Fe/molecule and that H-ferritin contains 24 identical subunits, an apparent ratio of 2 Fe/subunit can be calculated. However, if two Fe atoms were bridged by a single tyrosine, based on known model complexes, the extinction coefficients would be 320–900 $M^{-1}\ cm^{-1}\ Fe^{-1}$ (Murch et al., 1985, 1987). Moreover, bridging phenolates in Fe complexes give resonance Raman modes (Fe–OR–Fe) below 500 cm^{-1} (Murch et al., 1987), which are absent in the Fe(III)–tyrosinate complex in H-subunit-type ferritin (Waldo et al., 1993); the strong mode at 589 cm^{-1} observed in ferritin is most consistent with monodentate, terminal phenolate coordinated to Fe (Carrano et al., 1990). Thus, given the range of known extinction coefficients for Fe(III)–tyrosinate in proteins and the spectral properties of Fe(III)–tyrosinate in ferritin, it is likely that a single Fe atom is coordinated to a single tyrosine, with anywhere from 1 to 6 Fe atoms/site, involving 8–24 protein subunits.

Stoichiometry of Fe Oxidation. Two limiting cases for Fe/O_2 stoichiometry have been described for slow mineralizing horse spleen ferritin (Xu & Chasteen, 1991). At low ratios of Fe/protein, i.e., 24 Fe(II)/ferritin molecule, 2 Fe(II) are oxidized/O_2 consumed, with H_2O_2 being the product of O_2 reduction. At high ratios of Fe/protein, >200 Fe(II)/ferritin molecule, 4 Fe(II) are oxidized/O_2 consumed, with H_2O being the product of O_2 reduction (Xu & Chasteen, 1991; Sun & Chasteen, 1992).

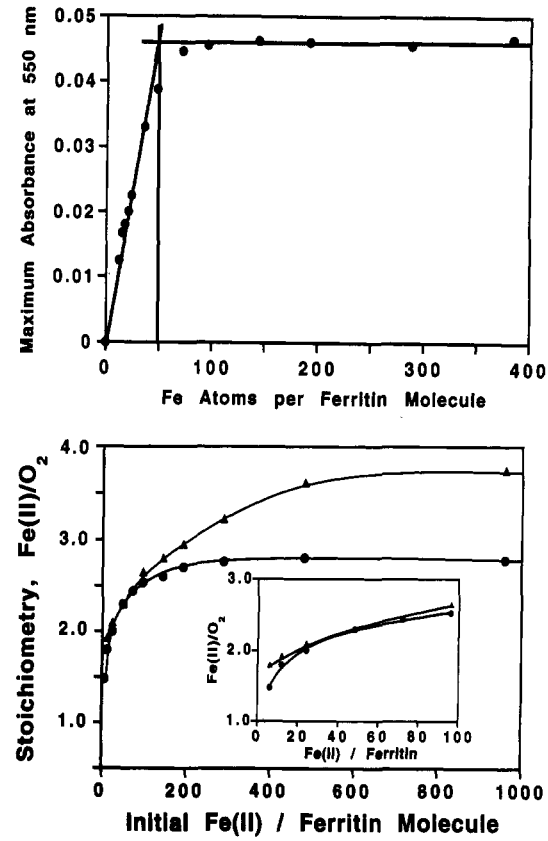

FIGURE 3: Stoichiometry of Fe(III)–tyrosinate formation and Fe(II) oxidation as a function of Fe(II) loading [Fe(II)/ferritin molecule]. (A, top panel) Fe(II)/ferritin molecule ratio required to saturate formation of Fe(III)–tyrosinate, determined by ultraviolet–visible stopped-flow spectroscopy. Reaction conditions were as described in Figure 1. For each ratio of Fe/protein, the maximum amount of Fe(III)–tyrosinate formed was determined from the maximum in the progress curve at 550 nm. (Depending on the Fe(II)/ferritin ratio, A_{550nm} reached a maximum ca. 1–3 s after mixing.) The drop-line at the intersection of lines fitted to the saturation curve indicates that a ratio of approximately 50 Fe(II)/ferritin molecule is required for saturation of the sites that form the Fe(III)–tyrosinate complex. (B, bottom panel) Stoichiometry of Fe(II) oxidation, Fe(II)/O_2, for horse spleen ferritin (▲) and H-subunit-type ferritin (●). Different Fe/protein ratios were achieved at constant concentrations of Fe(II) (1.0 × 10^{-4} M) by varying the protein concentration from 1.66 × 10^{-5} to 1.04 × 10^{-7} M. This ensured that the observed Fe/O_2 stoichiometries reflected changes in Fe(II)/ferritin ratios and not simply changes in [Fe(II)]. Other reaction conditions were as described in Figure 1. Stoichiometries of Fe(II) oxidation are similar for horse spleen and H-subunit-type ferritin at low Fe(II)/protein ratios; the Fe(II)/O_2 was ca. 2, indicating the production of H_2O_2. The two proteins display markedly different Fe(II) oxidation stoichiometries at higher Fe(II)/ferritin ratios. Fe(II)/O_2 approaches 4 for horse spleen ferritin at high Fe(II)/ferritin ratios, indicating that H_2O is the final product of O_2 reduction. In contrast, H-subunit-type ferritin ferroxidation produces substantial H_2O_2 at all ratios of Fe/protein. (This was confirmed by adding bovine liver catalase at the completion of oxidation, see Results.) (Inset) Data from panel B, rescaled to emphasize stoichiometry at low ratios of Fe/protein.

Measurement of O_2 consumed/Fe atoms oxidized was repeated for horse spleen ferritin (for comparison with H-subunit ferritin), and the range from ca. 2 Fe/O_2 at low Fe loadings to ca. 4 Fe/O_2 at high Fe loadings, previously observed by Xu and Chasteen (1991), was confirmed (Figure 3B). In contrast, for H-subunit-type ferritin the Fe/O_2 ratio

was always less than 2.8, indicating the production of some H_2O_2 even at high Fe/protein ratios. At ratios of Fe/protein of ca. 50, the Fe/O_2 ratio was ca. 2, indicating the predominance of H_2O_2 production when the major Fe(III) species formed was Fe(III)–tyrosinate (Figure 3B). The production of H_2O_2 during Fe(II) oxidation by H-subunit-type ferritin was confirmed at all ratios of Fe/protein by adding bovine liver catalase at the completion of oxidation; 30–50% of the O_2 consumed during ferroxidation was recovered depending on the Fe/ferritin ratio.[2]

Recovery of the Initial Burst of Oxidation. H-Subunit ferroxidation, as measured by O_2 consumption and Fe(III)–oxo multinuclear complex(es) formation, is clearly biphasic: a rapid burst followed by a slower phase (Figure 1A,B). Note that the H-type-subunit ferritin used here was isolated with no endogenous Fe, in contrast to previous studies in which Fe had to be removed before experiments. Since a rapid burst phase of oxidation had not been previously reported, the possibility existed that the rapid pathway and the ability to generate Fe(III)–tyrosinate, might be associated specifically with ferritin in which a mineral core had never formed. For example, ferritin might somehow be modified after the oxidation of the initial 50 Fe/molecule in such a way that the rapid pathway might be permanently abolished. To analyze the possibility that forming the iron mineral might permanently alter the rapid pathway, the recovery of the magnitude of the burst of oxidation and the capability of forming Fe(III)–tyrosinate was investigated. A sample of apoferritin in which the mineral core had never formed, was mixed with an initial bolus of Fe(II) (48 Fe/protein). At various times after mixing, samples were withdrawn, and a second bolus of Fe(II) was added (see Materials and Methods); progress curves were measured for oxygen consumption and Fe(III)–tyrosinate (A_{550nm}) formation. The magnitude of the burst of O_2 consumption and the amount of Fe(III)–tyrosinate formed for the second bolus of Fe(II) are shown as percentages relative to the values obtained for the addition of the first bolus of Fe(II) to apoferritin (Figure 4).

Clearly, the rapid pathway for Fe(II) oxidation by H-subunit ferritin is recoverable, as is the ability to form Fe(III)–tyrosinate. Although it is possible that formation of the Fe(III)–tyrosinate is unrelated to the major rapid biomineralization pathway in H-subunit ferritin, four observations make the possibility unlikely: first, Fe(III)–tyrosinate does not form unless a rapid burst of oxidation also occurs; second, the amount of Fe(III)–tyrosinate formed always corresponds to the magnitude of the burst, consistent with the recovery of a discrete number of sites on the protein for rapid Fe(II) oxidation; third, several types of H-subunit ferritin are now known to form an Fe(III)–tyrosinate complex (Waldo et al., 1993; Bauminger et al., 1993); fourth, it is clear that the magnitude of the burst and the amount of Fe(III)–tyrosinate formed recover at nearly identical rates (Figure 4). An inexplicable feature of the recovery of the sites forming Fe(III)–tyrosinate and the burst of oxidation is the lag in the early stage of recovery between the decay of Fe(III)–tyrosinate (A_{550nm}) and restoration of the sites for rapid oxidation. For example, during the first 40 s after the maximum formation of Fe(III)–tyrosinate at an Fe/protein ratio of 48, ca. 20% of the Fe(III)–tyrosinate (A_{550nm}) decreases (Figure 1C), but

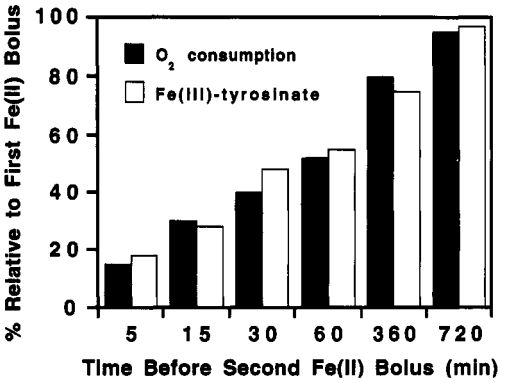

FIGURE 4: Recovery of the burst of O_2 consumption (■) and Fe(III)–tyrosinate formation (□) for the rapid ferroxidation pathway in H-subunit-type ferritin as a function of incubation time between the addition of two Fe(II) boluses. Values are percentages for the second Fe(II) bolus relative to the first Fe(II) bolus. Reaction conditions were as described in Figure 1. A bolus of 48 Fe(II)/ferritin molecule was added to H-subunit-type ferritin. At various times after mixing, samples of the ferritin were removed and treated with a second bolus of 48 Fe(II)/ferritin molecule, and progress curves were measured for O_2 consumption and Fe(III)–tyrosinate (A_{550nm}) formation. The burst of O_2 consumption was determined by fitting a line to the first 12 s of the second phase of each progress curve and extrapolating to the time of Fe(II) addition. The amount of Fe(III)-tyrosinate formed was determined as in Figure 3A. Note that recovery of the rapid oxidation pathway corresponded to the recovery of the site for Fe(III)–tyrosinate formation, consistent with the recovery of a discrete number of sites on the protein for rapid oxidation. The standard deviation of each data point was ≤10% of the value.

there is no detectable recovery of the burst of oxidation during this time interval—only the slow phase is observed. Instead, the sites reponsible for rapid mineralization and formation of Fe(III)–tyrosinate in H-subunit ferritin require ca. 5 min for 20% recovery and up to 12 h for full recovery. The initial lag between Fe(III)–tyrosinate decay and recovery of the burst suggests that an additional step beyond the decay of Fe(III)–tyrosinate is the rate-limiting step in the H-type subunit ferroxidation mechanism and that full restoration of the Fe(III)–tyrosinate site requires completion of one or more steps involving Fe beyond formation of the initial Fe(III)–tyrosinate complex. Given the complexity and directionality of ferritin biomineralization, it is not surprising that additional relaxations in the protein might be involved.

DISCUSSION

Fe(III)–tyrosinate appears to be the first of a series of Fe–protein complexes on the path of Fe through the protein coat from the solution outside ferritin to the solid, hydrous ferric oxide core inside ferritin. The sites along the path of Fe through the protein are not yet defined, although potential intermediates such as mono- and mixed-valence Fe–oxo dimers as well as Fe(III)–oxo clusters have been observed (Yang et al., 1987; Chasteen et al., 1985; Bauminger et al., 1989, 1991). One of the intermediate sites on the pathway of Fe through the protein coat may be the Glu^{58}/His^{61} ligands for Ca(II)/Tb(III) previously described (Lawson et al., 1991). Fe migration in ferritin is suggested by the relatively slow recovery of burst activity and ability to form Fe(III)–tyrosinate (Figure 4), as well as by the decrease of Fe(III)–tyrosinate with continuation of O_2 consumption and Fe(III)–oxo multinuclear complex formation. Evidence for Fe migration in ferritin during mineralization over long periods of time has been previously observed by measuring the EPR spectrum of vanadyl as a reporter of unoccupied Fe sites (Chasteen & Theil, 1982)

[2] The increase of O_2 at long times, after the completion of oxidation, is consistent with some spontaneous H_2O_2 disproportionation (Figure 1A). This could also explain, in part, the deviations from linearity during the latter part of the second phase of O_2 uptake (Figure 1A) compared to A_{420} formation (Figure 1B).

and by time-dependent changes in the ultraviolet–visible spectrum (A_{310nm}) (Treffry et al., 1984).

Differences in the ratio of Fe/O_2 for ferritin composed entirely of H-type subunits, compared to horse spleen ferritin (H:L = 0.15) displayed in Figure 3B might arise from the properties of H subunits in the ferritin molecule, which has been the explanation of differences previously observed (Levi et al., 1988; Lawson et al., 1988, 1991). One mechanism relates to possible differences in the type of Fe(III)–oxo clusters produced by H and L subunits in ferritin. If, for example, H subunits generated a large number of small Fe(III)–oxo clusters, such as that described by Taft et al., (1993) at specific protein catalytic sites, while L subunits produced a small number of larger, multinuclear Fe(III)–oxo clusters at less specific mineralization sites, the differences in stoichiometry of Fe/O_2 between H-subunit type ferritin and horse spleen ferritin (Figure 3B) could be explained.[3] Alternatively, a subset of H-subunit-specific ferroxidation sites might remain active throughout the Fe(II) oxidation process. Thus, oxidation on the core ($Fe/O_2 \sim 4$) and on the protein coat ($Fe/O_2 \sim 2$) might occur simultaneously during the second, slow phase of Fe(II) oxidation in ferritin comprised of H-type subunits, leading to the nonintegral Fe/O_2 stoichiometry at high Fe/protein ratios ($Fe/O_2 \sim 2.8$). Since such H-subunit-specific sites would be less important in horse spleen ferritin (H:L = 0.15), mineral-based oxidation ($Fe/O_2 \sim 4$) would determine the overall stoichiometry. Monomeric, 1-e^- oxidation of Fe(II) by O_2 has been suggested as one mechanism of ferroxidation in ferritin (Sun & Chasteen, 1992). Our observation of Fe/O_2 stoichiometries < 2, at Fe/protein ratios < 24, is consistent with some 1-e^- oxidation of Fe(II) (inset, Figure 3B). Such a notion is further supported by the increased stability of the Fe(III)–tyrosinate complex at very low Fe/protein ratios (12 Fe/protein; Figure 1C), by the increasing fraction of monomeric Fe(III) at low Fe/protein ratios as determined by EPR spin quantitation of the $g' = 4.3$ signal (Waldo et al., 1993), and by detection of a $g' = 2.0$ tyrosine-like radical by EPR spectroscopy (Waldo, Theil, and Huynh, unpublished observations). Oxidation of monomeric Fe(II) appears to occur preferentially at a site involving tyrosine, since the amount of Fe(III)–tyrosinate formed is directly proportional to added Fe, for Fe/protein ratios below 48 Fe/protein (Figure 3A). Another possible mechanism to explain the low Fe/O_2 stoichiometry might involve electron transfer from Fe(II) to tyrosine; however, such an explanation is less likely given the observation that no purple Fe(III)–tyrosinate is formed when Fe(II) is added anaerobically to H-subunit ferritin (Waldo et al., 1993).

The biphasic appearance of the O_2 uptake and A_{420} progress curves suggest a rapid preequilibrium phase followed by a "steady state" during which the rate of Fe(III)–oxo multinuclear complex(es) formation is constant. For ferritin, a simple explanation for the burst of oxidation followed by a slower, linear phase of oxidation would be the rapid accumulation, along a well-defined pathway for Fe migration, of an intermediate for which subsequent turnover is rate-limiting. Chymotrypsin provides a classic example of a burst arising from accumulation of a single protein-bound intermediate, during the hydrolysis of *p*-nitrophenyl ethyl carbonate (Hartley & Kilby, 1954). The acylenzyme is formed rapidly but hydrolyzes slowly. Progress curves for such systems resemble those for ferritin (Figure 1A,B) with an initial rapid pre-equilibrium phase during which stoichiometric amounts of enzyme-bound intermediates accumulate to steady-state concentration, followed by a slower phase during which further reaction with substrate is controlled by the rate of which enzyme-bound intermediates turn over to regenerate the active site. A burst occurs only when the rate of turnover of the intermediate is slow compared to its formation and is only detectable when enzyme and substrate are present at comparable concentrations. Both of these conditions are met by the Fe(III)–tyrosinate complex. However, a third condition, achieving steady-state concentration during the slow linear phase, does not occur in ferritin since Fe(III)–tyrosinate rapidly decreases during the initial "steady-state" phase of O_2 consumption and Fe(III)–oxo multinuclear complex formation (compare Figure 1, panels A, B, and C). Another, undetected intermediate might exist between Fe(III)–tyrosinate and the rate-limiting step in mineralization. Alternatively, the rapid and slow phases could represent two distinct pathways, where the rapid, Fe(III)–tyrosinate path may "prime" the slow path. For example, the protein-catalyzed rapid phase of Fe(II) oxidation could initiate the second, slower phase involving Fe(II) oxidation on small crystallites or mixed protein- ($Fe/O_2 \sim 2$) and mineral-catalyzed ($Fe/O_2 \sim 4$) Fe(II) oxidation. Finally, the 50 Fe(II) atom burst could represent the formation of small catalytic cluster(s), such as those described by Taft et al. (1993), perhaps bound to amino acid residues including tyrosine. Once such clusters attained a certain size, steric or energetic constraints could operate to shut off the rapid pathway, perhaps by blocking key residues or generating conformational changes in the protein structure. Subsequent movement of Fe to the final sites of greatest thermodynamic stability could act to free up the initial rapid path, perhaps by allowing the relaxation of the key protein residues to the initial conformation. Such a notion is consistent with the observation that the tyrosine residues which have been proposed as candidates for the Fe(III) complex (positions 25, 28, 30, and 133; Waldo et al., 1993) and the conserved Glu residues which have been suggested as Fe(III)–oxo cluster nucleation sites (Ford et al., 1984; Yang et al., 1987), are in close proximity to regions of considerable side-chain flexibility in the ferritin subunit structure (Harrison & Lilley, 1990; Trikha et al., 1993).

The burst of oxidation reported here represents a previously unappreciated aspect of ferritin ferroxidation, which must be incorporated into any mechanism of ferritin mineralization. It is an Fe(II) oxidation process of unprecedented rapidity in ferritin biomineralization. A $k_{ox} = 1000\ s^{-1}$ is comparable to typical product formation rate constants for enzyme-catalyzed reactions. The rapid formation of stoichiometric amounts of H-subunit-specific Fe(III)–tyrosinate during the burst in the formation of Fe(III)–oxo multinuclear complexes (Figure 1, Table I) requires a model for ferritin biomineralization which is more complex than any currently proposed. For example, the concerted 2-e^- transfer from O_2 to an Fe dimer proposed to occur at the Glu^{58}/His^{61} site (Treffry et al., 1992) does not explain the role of Fe(III)–tyrosinate, nor the fact that the Glu^{58}/His^{61} residues are present in ferritins exhibiting widely differing rates of mineralization (Waldo et al., 1993). Nor does a simple single Fe–protein interaction such as that proposed by Sun and Chasteen (1992) explain the burst of

[3] For example, large polycrystalline Fe(III)–oxo clusters could serve as alternative sites for Fe(II) oxidation (Macara et al., 1973; Crichton & Roman, 1978) with intermediate, partially reduced forms of O_2 (i.e., H_2O_2) remaining bound to the developing core and reacting with Fe^{2+} in a surface-diffusive manner, as previously suggested (Xu & Chasteen, 1991). Such two-dimensional diffusion would be less favorable on smaller crystallites which would have fewer sites for Fe binding.

oxidation (Figure 1), the sigmoidal rate plots (Figure 2), the stoichiometry of Fe oxidation (Figure 3B), or the slow rate of regeneration of both the rapid rate of O_2 consumption and formation of Fe(III)–tyrosine complex (Figure 4). A variety of mutant ferritins will be needed to fully understand the kinetics of Fe(III)–tyrosinate formation and to completely define the Fe path through the ferritin coat.

ACKNOWLEDGMENT

The authors are grateful to Dr. Carol Fierke for the use of the stopped-flow spectrophotometer.

REFERENCES

Bauminger, E. R., Harrison, P. M., Nowik, I., & Treffry, A. (1989) *Biochemistry 28*, 5486.
Bauminger, E. R., Harrison, P. M., Hechel, D., Nowik, I., & Treffry, A. (1991) *Biochim. Biophys. Acta 1118*, 48–58.
Bauminger, E. R., Harrison, P. M., Hechel, D., Hodson, N. W., Nowik, I., Treffry, A. & Yewdall, S. J. (1993) *Biochem. J.* (in press).
Carrano, C. J., Carrano, M. W., Sharma, K., Backes, G., & Loehr, J. S. (1990) *Inorg. Chem. 29*, 1865–1870.
Chasteen, N. D., & Theil, E. C. (1982) *J. Biol. Chem. 257*, 7672–7677.
Chasteen, N. D., Antanaitis, B. C., & Aisen, P. (1985) *J. Biol. Chem. 260*, 2926–2929.
Crichton, R. R., & Roman, F. (1978) *J. Mol. Catal. 4*, 75–82.
Dickey, L. F., Sreedharan, S., Theil, E. C., Didsbury, J. R., Wang, Y.-H., & Kaufman, R. E. (1987) *J. Biol. Chem. 262*, 7901.
Didsbury, J. R., Theil, E. C., Kaufman, R. E., & Dickey, L. F. (1986) *J. Biol. Chem. 261*, 949–955.
Fersht, A. (1975) *Enzyme Structure and Mechanism*, W. H. Freeman and Company, Reading and New York.
Ford, G. C., Harrison, P. M., Rice, D. W., Treffry, A., Smith, J. M. A., White, J. L., & Yariv, J. L. (1984) *Philos. Trans. R. Soc. London, B 324*, 551–565.
Hanna, P. M., Chasteen, N. D., Rottman, G. A., & Aisen, P. (1991) *Biochemistry 30*, 9210–9216.
Hartley, B. S., & Kilby, B. A. (1954) *Biochem. J. 56*, 288.
Harrison, P. M., & Lilley, T. H. (1990) in *Iron Carriers and Iron Proteins* (Loehr, T. M., Ed.) pp 353–452, VCH, Weinheim and New York.
Hill, A. V. (1910) *J. Physiol. (London) 40*, 190.
Jacobs, D. L., Watt, G. D., & Frankel, R. B. (1989) *Biochemistry 28*, 1650.
Johnson, K. A. (1986) *Methods Enzymol. 134*, 677–705.
Lawson, D. M., Treffry, A., Artymiuk, P., Harrison, P. M., Yewdall, S. J., Luzzago, A., Cesareni, G., Levi, S., & Arosio, P. (1989) *FEBS Lett. 254*, 207–210.
Lawson, D. M., Artymiuk, P. J., Yewdall, S. J., Smith, J. M. A., Livingstone, J. C., Treffry, A., Luzzago, A., Levi, S., Arosio, P., Cesareni, G., Thomas, C. D., Shaw, W. V., & Harrison, P. M. (1991) *Nature 349*, 541–544.
Levi, S., Luzzago, A., Cesareni, G., Cozzi, A., Fransecshinelli, F., Albertini, A., & Arosio, P. (1988) *J. Biol. Chem. 263*, 1802–1806.
Levi, S., Salfield, J., Fransecshinelli, F., Cozzi, A., Dorner, M., & Arosio, P. (1989) *Biochemistry 28*, 5179–5184.
Lowry, O. H., Rosebrough, N. J., Farr, A. L., & Randall, R. J. (1951) *J. Biol. Chem. 193*, 265–275.
Macara, I. G., Hoy, T. G., & Harrison, P. M. (1973) *Biochem. J. 135*, 343–348.
Mackle, M., Garner, C. D., Ward, R. J., & Peters, T. J. (1991) *Biochim. Biophys. Acta 1115*, 145–150.
Mann, S., Williams, R. J. P., Treffry, A., & Harrison, P. M. (1987) *J. Mol. Biol. 198*, 405–416.
Murch, B. P., Boyle, P. D., & Que, L., Jr. (1985) *J. Am. Chem. Soc. 107*, 6728.
Murch, B. P., Bradley, F. C., Boyle, P. D., Papaefthymiou, V., & Que, L., Jr. (1987) *J. Am. Chem. Soc. 109*, 7993–8003.
Que, L., Jr. (1983) *Coord. Chem. Rev. 50*, 73.
Rohrer, J. S., Joo, J. S., Dartyge, E., Sayers, D. E., Fontaine, A., & Theil, E. C. (1987) *J. Biol. Chem. 263*, 18339–18344.
Rohrer, J. S., Frankel, R. B., Papaefythmiou, G. C., & Theil, E. C. (1989) *Inorg. Chem. 28*, 3393–3395.
Rohrer, J. S., Islam, Q. T., Watt, G. D., Sayers, D. E., & Theil, E. C. (1990) *Biochemistry 29*, 259–264.
Segel, I. H. (1975) *Enzyme Kinetics—Behavior and Analysis of Rapid Equilibrium and Steady-State Enzyme Systems*, John Wiley & Sons, Inc., New York.
Sun, S., & Chasteen, N. D. (1992) *J. Biol. Chem. 267*, 25160–25166.
Taft, K. L., Papaefthymiou, G. C., & Lippard, S. J. (1993) *Science 259*, 1302–1305.
Theil, E. C. (1987) *Annu. Rev. Biochem. 56*, 289–315.
Theil, E. C. (1990) *Adv. Enzymol. Relat. Areas Mol. Biol. 63*, 421–449.
Theil, E. C. & Sayers, D. E. (1991) *Iron Biomineralization*, pp 295–306, Plenum Press, New York.
Treffry, A., & Harrison, P. M. (1984) *J. Inorg. Biochem. 21*, 9–20.
Treffry, A., Hirzmann, J., Yewdall, S. J., & Harrison, P. M. (1992) *FEBS Lett. 302*, 108–112.
Trikha, J., Waldo, G. S., Lewandowski, F., Ha, Y., Theil, E. C., Weber, P., & Allewell, N. (1993) *Proteins* (in press).
Wade, V. J., Levi, S., Arosio, P., Treffry, A., Harrison, P. M., & Mann, S. (1991) *J. Mol. Biol. 221*, 1443–1452.
Waldo, G. S., Ling, J., Sanders-Loehr, J., & Theil, E. C. (1993) *Science 259*, 796–798.
Xu, L. B., & Chasteen, N. D. (1991) *J. Biol. Chem. 266*, 19965–19970.
Yablonski, M. J., & Theil, E. C. (1992) *Biochemistry 31*, 9680.
Yang, C. Y., Meagher, A., Hunyh, B. H., Sayers, D. E., & Theil, E. C. (1987) *Biochemistry 26*, 497.